Jakub DAWIDZIUK

Politechnika Białostocka, Wydział Elektryczny

Power Losses in PWM Inverters using Silicon Carbide Devices

Streszczenie. *W artykule są badane straty mocy w falownikach PWM z przyrządami SiC. Straty mocy są określane poprzez modelowanie w różnych warunkach obciążenia. Do oceny strat przewodzenia używany jest uproszczony model przyrządu stanowiący szeregowe połączenie źródła napięcia i rezystora. Wyniki badań eksperymentalnych potwierdzają założenia teoretyczne.* ***(Straty mocy w falowniku PWM z przyrządami półprzewodnikowymi z węglika krzemu).***

Abstract. *In this paper the power losses in PWM-VSI inverters using SiC devices are investigated. The power losses are determined by simulation based on the loss models for different load conditions. For the conduction loss evaluation the device models simplified to a voltage source in series with a resistor. Theoretical models are correlated well with the experimental data.*

Słowa kluczowe: falownik PWM, straty mocy, przyrządy półprzewodnikowe SiC, modelowanie.
Keywords: PWM inverter, power losses, SiC devices, modelling.

Introduction

Presently, almost all the power electronics converter systems in applications use silicon (Si) based power semiconductor switches. The performance of these systems is approaching the theoretical limits of the Si material. Another material, silicon carbide (SiC) with its superior properties compared with Si, is a good candidate to be used in the next-generation power devices.

SiC comes in different crystalline structures or polytypes. The two most common polytypes are 6H-SiC and 4H-SiC. First 6H-SiC was available; then 4H-SiC was introduced around 1994, and it deflected interest from 6H-SiC for high-power applications.

Until today, MOSFETs and IGBTs are the first choice for switching devices in power electronic circuits for most applications. Typical applications are inverters for driving electrical machines or rectifiers feeding the grid from renewable energy sources or power supplies. For these applications there is a demand for more efficient inverters. There are different ways to achieve this. One way is to use power semiconductor devices with good conducting behaviour to reduce the losses during on-state. In this case the devices designed in this way have a bad switching performance meaning high switching losses that leads to low switching frequencies and hence to large filters creating losses as well. Another approach is to use devices with good switching performance so that high switching frequencies and small filters are possible. However in this case the conducting losses increase and the system efficiency is reduced as well.

In recent years new promising devices which seem to overcome the disadvantages mentioned above and combine the advantages of silicon MOSFETs and IGBTs are under investigation and start to be introduced into the market. To achieve this, the substrate of these devices is no longer silicon but silicon carbide is used. Different companies intensify their research effort on silicon carbide switches.

Advantages of SiC compared with Si

Silicon carbide power electronic devices are expected to have better characteristics than their silicon counterparts once processing and packaging issues have been solved. SiC power devices bring great performance improvements. Some of these advantages compared with Si based power devices are as follows:

- SiC power devices have lower on-resistances $R_{DS,on}$. With lower resistances, SiC devices have lower conduction losses and therefore higher overall efficiency.
- SiC-based power devices have higher breakdown voltages.
- SiC has a higher thermal conductivity and thus a lower junction-to-case thermal resistance, R_{th-jc} and thus device temperature increase is slower.
- SiC can operate at high temperatures at up to $300^0 C$ [1]. Si devices can operate at a maximum junction temperature of only $175^0 C$.
- SiC is extremely radiation hard; i.e., radiation does not degrade the electronic properties of SiC.
- Forward and reverse characteristics of SiC power devices vary only slightly with temperature and time, they are more reliable.
- SiC power devices have excellent reverse recovery characteristics. With less reverse recovery current, the switching losses and EMI are reduced and there is less or no need for snubbers.

Availability of high-temperature power devices will promote R&D activities of their applications in high-temperature environment demanding further research in control electronics, passive components, renewable energy sources, and nuclear power. Hence, power electronics that are based on large band-gap devices will bring a renaissance in the future, particularly in a high-power area.

The power losses in semiconductor devices can be divided into static on-resistance losses, leakage losses at reverse blocking voltages, and dynamic switching losses.

The static on-resistance losses mainly contain the resistive loss in the lowly-doped drift region, added to device specific resistance contributions such as for example the contact resistance. The specific on-resistance of the drift region is $R_{on} = 4V_{BD}^2 / \varepsilon\mu E_B^3$, where the denominator is Baliga's figure-of-merit [2], which is a combination of several materials parameters important for the operation of a device in a certain application. For example, using Baliga's figure-of-merit, SiC would be 120 times better than Si for use in power devices.

Static Model for SiC power Schottky diodes

The equivalent circuit of a SiC Schottky diode consists connected in series of the voltage drop across the Schottky barrier V_{FB}, the specific series resistance of the lightly doped drift region R_D, and the resistances of substrate R_S and contact R_C. R_D is proportional to a power of the

temperature. This is because $R_D = 1/\mu_n$ and $\mu_n \propto 1/T^{\gamma}$. Thus, $R_D \propto T^{\gamma}$ where γ is a constant and is 2.42 for Si and 1.3 for 6H-SiC at 300K. Under the forward bias condition the current flow across the Schottky barrier is given by

$$I_F = ACT^2\left[exp\left(\frac{q}{kT}\left(V_{FB}-\phi_B\right)\right)\right], \quad (1)$$

where: A is the device effective area, C is the Richardson's constant, T is the absolute temperature, q is the charge of an electron, k is the Boltzmann's constant, ϕ_B is the Schottky barrier height between the metal and semiconductor. For 4H-SiC, the value of the Richardson's constant is 146 A·cm^{-2}·K^{-2} [3].

Neglect R_S and R_C (because they are small in comparison with R_D), solve (1) for V_{FB} the total voltage drop across a Schottky power diode can be expressed as

$$V_F = \phi_B + \frac{kT}{q} ln\left(\frac{I_F}{ACT^2}\right) + I_F R_D . \quad (2)$$

Differentiation of (2) with respect to I_F yields the on-state specific resistance:

$$R_{sp} = \frac{dV_F}{dI_F} = \frac{kT}{q}\left(\frac{1}{I_F}\right) + R_D \approx R_D . \quad (3)$$

For forward currents greater than 1 A the first component in (3) may be neglected, because most SiC Schottky power diodes operate in this region.

The voltage drop on the diode and the series resistance are the sources of a diode's conduction losses. These losses can be expressed as:

$$P_{CD} = I_{D,ave} V_D + I^2_{D,rms} R_D , \quad (4)$$

where: $I_{D,ave}$ and $I_{D,rms}$ are the average and rms value of the current flowing through the diode, respectively.

When a dc current I_{DC} is applied, then both the average current and rms current are equal to the dc carrent and (4) becomes

$$P_{CD} = I_{DC} V_D + I^2_{DC} R_D . \quad (5)$$

From (5), it is clear that resistive losses dominate the conduction losses for the dc operation especially at higher current values.

Dynamic model for SiC power Schottky diodes

Although the reverse recovery current is much smaller for Schottky diodes than that of pn diodes, the reverse recovery loss dominates its switching losses. Figure 1 shows the typical turn-off waveforms of a diode. In this model only reverse recovery loss is considered.

The reverse recovery loss of a diode can be calculated as follows [4]:

$$P_{rr} = f_s \frac{BV}{2S}\left(\frac{di_R}{dt}\right)\left(\frac{St_{rr}}{S+1}\right)^2 , \quad (6)$$

where BV is the applied reverse voltage.

The switching loss for SiC Schottky diode is almost independent of the change in temperature. The reverse recovery current is dependent on charge stored in the drift region. The SiC Schottky diode has no stored charge because it is a majority carrier device, and hence has virtually constant turn on energy loss for a wide temperature

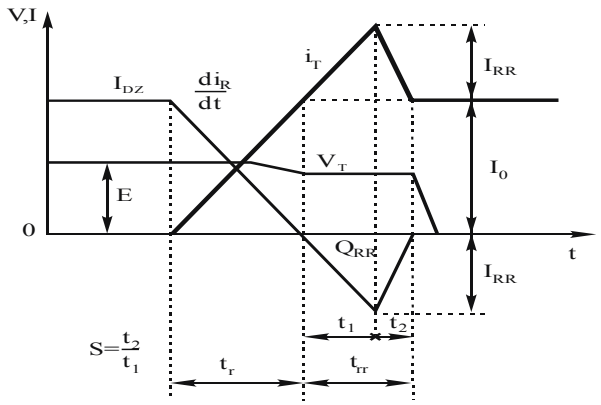

Fig. 1. Voltage and current waveforms for a power diode driven by currents with a specified rate of fall during turn-off

range. The negligible reverse recovery current reduces the oscillation due to ringing and also eliminates the need for a snubber for limiting the reverse recovery. This results in increased efficiency as the losses are minimized. The reduced blocking layer thickness, due to the high electric breakdown field of the SiC material, contributes to the low switching losses of the SiC diode.

Models for SiC JFET and MOSFET

The on-state resistance of SiC JFET and MOSFET is mainly composed of channel, substrate, contact, and drift region resistances. For high power devices it is dominated by drift region resistance. Then the other components can be neglected. For SiC JFETs and MOSFETs, the conduction loss is mainly caused by on-state resistance, R_{on}. It is calculated by

$$P_C = I^2_{rms} R_{DS,on} , \quad (7)$$

where I_{rms} is the effective current flowing in the device.

The switching losses can be calculated using piece-wise linear turn-on and turn-off waveforms. This is an approximation, which does not consider the physics behind the switching. The turn-on and turn-off energy loss equations are derived in [5] as

$$E_{on} = \frac{1}{3\left(K_1 - 1\right)} \varepsilon_s E_C^V \sqrt{\frac{V}{BV}} , \quad (8)$$

$$E_{off} = \frac{1}{3\left(K_2 + 1\right)} \varepsilon_s E_C^V \sqrt{\frac{V}{BV}} , \quad (9)$$

$$K_1 = \frac{g_m\left(V_{GH} - V_{TH}\right)}{J}, K_2 = \frac{g_m\left(V_{TH} - V_{GL}\right)}{J} , \quad (10)$$

where: ε_s is the permittivity of semiconductor, E_C is the avalanche electric breakdown field, BV is the breakdown voltage, E_{on} and E_{off} are the turn-on and turn-off losses (J/cm^2), g_m is the transconductance, J is the current

density, V_{GH}, V_{GL} are highest and lowest applied gate voltages, and V_{TH} is the threshold voltage. These capacitances are charged and discharged by effective currents of $(K_1 - 1)J$, and $(K_2 + 1)J$, respectively.

For the switching frequency f_S the total switching losses $E_{tot} = E_{on} + E_{off}$ can be given by

$$P_{ST} = f_S E_{tot} = \frac{1}{3} f_S \varepsilon_r E_C V \sqrt{\frac{V}{BV}} \left(\frac{1}{K_1} + \frac{1}{K_2} \right), \quad (11)$$

where P_{ST} is switching power loss density [W/cm^2].

Estimating device power loss in inverter

Examining device efficiency and current utilisation level in a PWM inverter, rather than the more common test set-up of a single-ended chopper, involves greater analytical complexity because device current and duty-cycle vary sinusoidal, and the variation in all loss components with current level must be determined and averaged over an output-frequency f_0 period. The averaging, however, becomes relatively simple with high carrier-frequency ratio p [i.e. p or $f_S / f_0 \geq 10$], provided conduction power-loss and switching energy-loss equations can be expressed as continuous functions of current, because discrete-equation averages may then be approximated by closed-form continuous-equation averages.

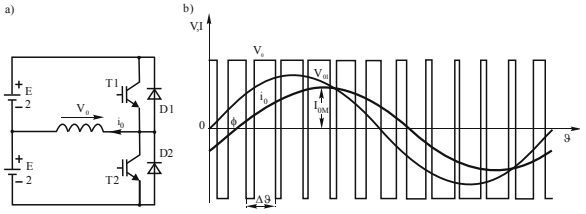

Fig. 2. Equivalent circuit for power loss estimation, PWM voltage, its fundamental component, and lagging output current

The power-loss in each of the bridge-legs of a 3-phase inverter is the same, assuming steady-state machine on, and it is only necessary to examine the equivalent circuit for one bridge-leg and load-phase shown in Fig. 2. Also, the inductive load, i.e. the machine-winding, is assumed to draw a pure sinusoidal current since the inverter switching period is usually chosen to be far less than the winding time-constant to give low current-ripple.

The method of solution, although inherently less flexible and accurate, avoids the need to generate such complex algorithms for numerical solution by computer, and has been shown to give surprisingly low error for regular-sampled-PWM, provided p is at least 10.

Conduction power loss

In order to determine the conduction loss, a simplified device model is employed. The simplified models for JFET, MOSFET, and diode are expressed in (12a) and (12b) respectively

$$V_{DS} = i_0 R_{DS,on}, \quad (12a)$$

$$V_{AK} = V_{0D} + i_0 R_D, \quad (12b)$$

where voltages V_{DS} and V_{AK} represent the on-state voltage drops of transistors and diode, V_{0D} is voltage drop at zero current condition, i_0 is the device current. The resistive elements are assumed to be linear, $R_{DS,on}$ and R_D are the resistive elements of transistors and diode.

Bridge-leg current at any instant ϑ of the fundamental output period is given by

$$i_0(\upsilon) = I_{0M} \sin(\vartheta - \phi), \quad (13)$$

where I_{0M} is peak output current, $\vartheta = \omega t$, and ϕ is the phase difference between the load current and PWM voltage waveform fundamental.

Approximate value of pulse-width , at high carrier-frequency ratio, can be determined from

$$\frac{U_{n\max} - u_m}{U_{n\max}} = \frac{\Delta\vartheta_D / 2}{\Delta\vartheta / 4}. \quad (14)$$

Defined as: $m_a = U_{n\max} / Um\max$ the amplitude modulation ratio, $u_m = U_{m\max} \sin \omega_0 t$ instantaneous value of the control signal, $\Delta\vartheta = 2\pi / p$ carrier frequency period obtained transistor and diode normalized periods at any ϑ are given by

$$\Delta\vartheta_T = \frac{1}{2}(1 + m_a \sin\vartheta)\Delta\vartheta, \quad (15a)$$

$$\Delta\vartheta_D = \frac{1}{2}(1 - m_a \sin\vartheta)\Delta\vartheta. \quad (15b)$$

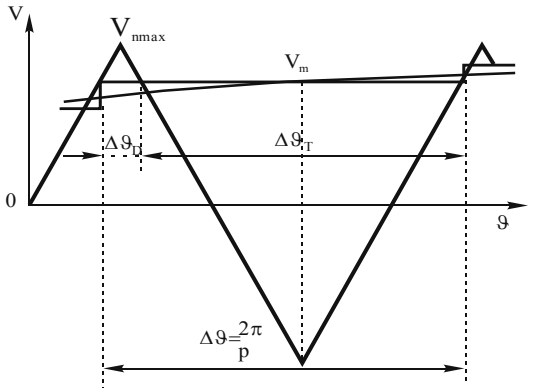

Fig. 3. Extrapolation of the average value voltage

Therefore, net average conduction power-loss over 2π is given by

$$P_{CT} = \frac{1}{2\pi} \sum_{s=\phi/\Delta\vartheta}^{(\pi+\phi)/\Delta\vartheta} \left[R_T i_0{}^2 (s\Delta\vartheta) \right] \Delta\vartheta_T, \quad (16a)$$

$$P_{CD} = \frac{1}{2\pi} \sum_{s=\phi/\Delta\vartheta}^{(\pi+\phi)/\Delta\vartheta} \left[U_{0D} i_0 (s\Delta\vartheta) + R_D i_0{}^2 (s\Delta\vartheta) \right] \Delta\vartheta_D. \quad (16b)$$

Approximate closed-form solutions are obtained by assuming $\Delta\vartheta$ tends to zero and using continuous system averages given by

$$P_{CT} \approx \frac{1}{2\pi} \int_{\phi}^{\pi+\phi} R_T i_0^2(\upsilon) \frac{1 + m_a \sin\vartheta}{2} d\vartheta, \quad (17a)$$

(17b) $P_{CD} \approx \frac{1}{2\pi}\int_{\phi}^{\pi+\phi}\left[U_{0D}i_0(\vartheta)+R_D{i_0}^2(\vartheta)\right]\frac{1-m_a\sin\vartheta}{2}d\vartheta$.

These, when solved, give the following switch and diode average conduction power-loss equations

(18a) $$P_{CT} \approx I_{0M}^2 R_T\left(\frac{1}{8}+\frac{m_a}{3\pi}\cos\phi\right),$$

(18b) $$P_{CD} \approx \frac{1}{2}I_{0M}U_{0D}\left(\frac{1}{\pi}-\frac{m_a}{4}\cos\phi\right)+I_{0M}^2 R_D\left(\frac{1}{8}-\frac{m}{3\pi}\cos\phi\right).$$

Although these loss equations do not incorporate the effects of third-harmonic addition, which is later assumed to be used, the difference in loss may be shown to be small.

Switching power loss

Switching loss comprises turn-on and turn-off loss components. The heat energy added at each switching interval is now readily measurable with high-bandwidth digital oscilloscopes, which perform waveform multiplication and integration to give instantaneous power energy change, and increasingly graphs of switching energy versus current are being supplied by device manufacturers. Wherever possible, such direct loss measurements are used. For those devices for which loss data are unavailable, the switching energy is estimated from switching time data.

Turn-off switching energy

Power-device switching performance is often estimated from turn-off current fall. Experimental and published switching waveforms generally show that 50% or more of the turn-off loss occurs during the voltage rise with high-voltage devices. In the case, where the switching crossover time measurements, $\left(t_{c(off)} \neq t_s + t_f\right)$ are unavailable, Eq. (19a) may be used for loss estimation

(19a) $$E_{SW(off)}(\vartheta) = \frac{1}{2}EI_0(\vartheta)\frac{t_{c(off)}}{0.8} = EI_0(\vartheta)\frac{t_f}{0.8},$$

where, $I_0(\vartheta)$ is a value of the switched current at any instant ϑ. The 0.8 factor arises due to measurement at 10 or 90% levels.

The average turn-off power losses can be obtained by averaging of instantaneous power losses over one fundamental cycle

(19b) $$P_{S(off)} = \frac{t_f f_s E I_{0M}}{0.8\pi}.$$

Where switching energy-loss measurements do exist (Fig. 4), the relationship between $E_{ST(off)}$ and switched current at any instant may be approximated by Eq. (20a) in many cases, where E_{TR} is the turn-off energy-loss at reference current value I_{TR} [6]

(20a) $$E_{TSW(off)}(\vartheta) = \left(\frac{I_0(\vartheta)}{I_{TR}}\right)^n E_{TR},$$

where *n* is the gradient of the loss graph when plotted on logarithmic axes

(20b) $$n = \frac{\log\left(E_{off\,2}\right)-\log\left(E_{off\,1}\right)}{\log\left(I_{off\,2}\right)-\log\left(I_{off\,1}\right)}.$$

With sinusoidal modulated current the total average power-loss is given by

(21a) $$P_{ST(off)} = \frac{f_s}{2\pi}\left(\frac{I_{0M}}{I_{TR}}\right)^n E_{TR}\int_0^{\pi}\sin^n\vartheta d\vartheta,$$

(21b) $$P_{ST(off)} = \frac{f_s}{2\pi}\left(\frac{I_{0M}}{I_{TR}}\right)^n E_{TR}\frac{\pi}{n2^{n-2}}\frac{\Gamma(n)}{\left[\Gamma\left(\frac{1}{2}n\right)\right]^2}.$$

It should be noted that the derived loss equations are merely examples, and their form, as well as their coefficients, may be adjusted for greater accuracy or new devices.

Turn-on switching energy

The variation in turn-on energy-loss with current, $E_{ST(on)}$ may be approximated by Eq. (20a).

When a graph of $E_{ST(on)}$ measurements is available, and a parabolic-curve approximation to it using Eq. (22) is possible, $P_{ST(on)}$ is obtained by averaging Eq. (22) over 2π to give Eq. (23), as previously performed for $P_{ST(off)}$

(22) $$E_{TSW(on)}(\vartheta) = \left(\frac{I_{0M}}{I_{DR}}\sin\vartheta\right)^m E_{DR},$$

(23) $$P_{ST(on)} = \frac{f_s}{2\pi}\left(\frac{I_{0M}}{I_{DR}}\right)^m E_{DR}\int_0^{\pi}\sin^m\vartheta d\vartheta = \frac{f_s}{2\pi}\left(\frac{I_{0M}}{I_{DR}}\right)^m E_{DR}\frac{\pi}{m2^{m-2}}\frac{\Gamma(m)}{\left[\Gamma\left(\frac{1}{2}m\right)\right]^2}.$$

When directly measured $E_{ST(on)}$ date is unavailable, turn-on switching energy may be estimated using diode reverse-recovery charge Q_{rr}.

With a stiff drive circuit and little series parasitic-inductance, switch turn-on waveforms, with current freewheeling in a fast-recovery diode, are similar to those in Fig. 1, where Q_{rr} is assumed to be fully discharged while the switch voltage v_T, is high at approximately E. Turn-on switching energy may then estimated from

(24a) $$E_{ST(on)}(\vartheta) = \int_0^{t_r+t_{rr}} v_T i_T dt = E\left[\begin{array}{l} Q_{RR}+\frac{1+2S}{1+S}I_0(\vartheta)\sqrt{\frac{Q_{RR}(1+S)}{2(di_R/dt)}}+ \\ +\frac{1}{2}\left(I_0(\vartheta)+\sqrt{\frac{2Q_{RR}(di_R/dt)}{S+1}}\right)t_r \end{array}\right],$$

where: $S = t_2/t_1$ is "snappiness" factor as functions of the time rate of change of the reverse current.

Assuming $t_1 = t_2$ and $t_r = I_0/(di_R/dt)$ Eq. (13a) can be rewritten as

(24b) $$E_{TSW(on)}(\vartheta) = E\left(Q_{RR}+2I_0(\vartheta)\sqrt{\frac{Q_{RR}}{di_R/dt}}+\frac{I_0^2(\vartheta)}{2di_R/dt}\right).$$

With modulated current energy-loss $E_{TSW(on)}$ must be averaged over an output frequency period. Recovery di/dt is assumed sufficiently high, such that Q_{RR} approaches the total stored charge in the diode, and is approximately proportional to forward current

(25a) $$Q_{RR}(\vartheta) = \frac{I_0(\vartheta)}{I_{DR}} Q_{RI},$$

and for sine-weighted PWM at each switching instant ϑ

(25b) $$Q_{RR}(\vartheta) = \frac{I_0(\vartheta)}{I_{DR}} Q_{RI} \sin\vartheta,$$

where Q_{RI} is the recovered charge at a reference current I_{DR}.

With sinusoidal load-current turn-on switching losses at any switching instant is given by

(26) $$P_{ST(on)}(\vartheta) = f_s E \left(\begin{array}{l} \frac{I_{0M}}{I_{DR}} Q_{RI} \sin\vartheta + \\ + 2 I_{0M} \sin^{\frac{3}{2}}\vartheta \sqrt{\frac{(I_{0M}/I_{DR}) Q_{RI}}{di_R/dt}} + \\ + \frac{I_{0M}^2}{2 di_R/dt} \sin^2\vartheta \end{array} \right),$$

which gives Eq. (27) when averaged over 2π

(27) $$P_{ST(on)} \approx f_s E \left(\begin{array}{l} \frac{Q_{RI}}{\pi} \frac{I_{0M}}{I_{DR}} + \frac{I_{0M}^2}{8 di_R/dt} + \\ + 0.556 I_{0M} \sqrt{\frac{Q_{RI} I_{0M}/I_{DR}}{di_R/dt}} \end{array} \right).$$

Total power losses

The total conduction and switching losses produced by a bridge-leg switch-diode pair, may be calculated by collecting power-loss terms

(28) $$P_{tot} = P_T + P_D = \left(P_{CT} + P_{ST(on)} + P_{ST(off)}\right) + P_{CD},$$

and produced by a inverter

(29) $$P_{TOT} = 6 P_{tot}.$$

Test circuit

The test circuit shown in Fig. 4 was used for testing different types of semiconductor devices in several configurations.

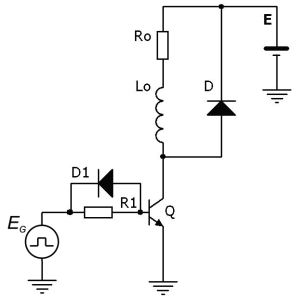

Fig. 4. Simplified schematic diagram of switching and conducting losses of diodes and transistors measurement system

Devices were tested for both static and dynamic characteristics at room temperature. The switching waveforms of the devices at the test condition were 95 V, 5 A and 25 ^{0}C they can be seen at Figs. 5(a) and (b). Their switching energy losses at different current level are shown in Fig. 6. All the switching losses increase with increasing current and switching frequency.

a) b)

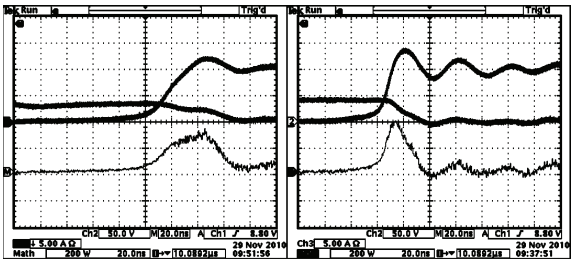

Fig. 5. Waveforms of voltage, current and power during turn-off a) IGBT (IXGH32N60BUT) with freewheeling diode SiC(C2D20120), b) MOSFET (IRFP27N60K) same diode SiC(C2D20120)

Experimental verification of the loss estimation

In the experiment the hard switching inverter was utilized for measuring the power losses. The 5th generation IGBT module CM100DY-24NF (1200V, 100A with low turn-off energy) Mitsubishi Electric, silicon carbide power diode SDP20S120D, and normally-off trench silicon carbide power JFET SJEP120R063 SemiSouth were used as the main switching devices of the inverter circuit. The power losses were measured under the following conditions: DC source voltage $E = 300V$, output currents $I_0 = 3, 5, 9, 12, 15, 18\,A$ and switching frequency $f_s = 10\,kHz$. The inductive load has been built by using an E65/32/27-3F3 core. The gate driver of the IGBTs is a M57160AL.

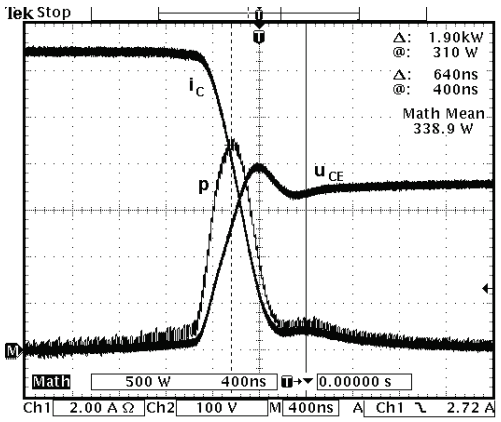

Fig. 6. Experimentally hard switching turn-off waveforms: i_C - collector current, u_{CE} - collector-emitter voltage, and p - power losses

The experimental collector-emitter voltage, collector current waveforms and switching losses of the IGBT have been measured with Tektronix equipments: the high voltage probe model P5100 (2.5 kV, 250 MHz), the current probe model A6312 (20 A, 100 MHz) and the oscilloscope model TDS 3014, respectively.

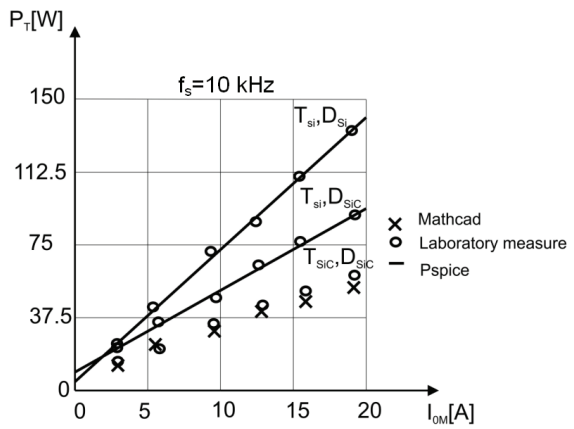

Fig. 7. Total power losses as a function of load current in hard-switched inverter (HSI) with Si and SiC

The simulation results of the analysis obtained by using the Spice model of the IGBT and Mathcad model of SiC JFET were compared to the characteristics obtained by measurements.

In Fig. 7 the total losses as a function of load current of an Si hard-switched and SiC hard-switched inverters are shown. The calculated values of the power losses are well agreed with the experimental results. Therefore, the validity of this analysis is confirmed. As can be seen from these curves the difference between Si (HIS) and SiC (HIS) rises with an increase of conduction current. The superior switching performance of the diodes and transistors improves the efficiency of the inverter and also impacts the main power switches by reducing the stress on them and thus improving system performance. A performance comparison of the all-Si, the hybrid inverter and all-SiC is shown in Figure 7. The hybrid inverter and all-SiC inverter losses are lower than the all-Si inverter for all operating currents. The results show up to 33% and 60% reduction in the losses.

Conclusions

In this paper, losses of an of a Si-based PWM inverter and a SiC-based PWM inverter are compared. Replacing Si-based power devices with SiC-based power devices brings many advantages for power conversion applications. The advantages of SiC based power electronics were discussed in previous section. The result of the loss studies showed an increase in efficiency with a decrease in the device losses when SiC is used. In addition, thermal studies showed that SiC-based converters need less cooling because of the material's superior thermal characteristics and because of lower losses associated with SiC power devices. When the processing issues are solved and the price of SiC wafers decreases, it is expected that SiC will replace Si in power devices, especially in medium to high-voltage range. SiC diodes and transistors are being used in niche applications such as power factor correction circuits or as antiparallel (free-wheeling) diodes in inverters. It is expected that the first impact of SiC devices on inverters will be as a result of SiC Schottky diodes replacing the conventional Si pn diodes.

Acknowledgements. *The project was financed by the National Science Center No. N N510 512040.*

REFERENCES

[1] Richmond J., Hull B., Ryu S. H., Agarwal A., Palmour J., and Scofield J., Reliable Silicon Carbide MOSFET Operation at 300^0 C Junction Temperature, *Proceedings of the International High Temperature Electronics Conference,* Albuquerque, NM, May 12-15, (2008), pp. 109-112

[2] Baliga B.J., Power semiconductor device figure of merit for high-frequency applications, *IEEE Electron Device Letters* (1989)Vol. 10, No. 10, pp. 455-457

[3] Roccaforte F., Libertino S., Giannazzo F., Bongiorno C., Via F. L., and Raineri V., Ion irradiation of inhomogeneous Schottky barriers on silicon carbide, *Journal of Applied Physics*, (2005), vol. 97, issue 12

[4] Baliga B. J., Modern Power Devices, John Wiley&Sons Inc., New York, (1987)

[5] Huang Q., and Zhang B., Comparing SiC Switching Power Devices: MOSFET, NPN Transistor, and GTO Transistor, *Solid State Electronics*, (2000) Vol. 44, No. 2, pp. 325-340

[6] Dawidziuk J., Analiza strat mocy w biegunowych falownikach napięcia, *Wydawnictwo Politechniki Białostockiej*, 2002.

Autor*: dr hab. inż. Jakub Dawidziuk prof. PB, Politechnika Białostocka, Wydział Elektryczny, ul. Wiejska 45D, 15-351 Białystok, E-mail: dawid@pb.edu.pl.*